BENTHAM
SCIENCE

Oral Triphenylmethane Food Dye Analog, Brilliant Blue G, Prevents Neuronal Loss in APPSwDI/NOS2^{-/-} Mouse Model

Jacob A. Irwin^a, Alev Erisir^{b,*} and Inchan Kwon^{a,c,*}

Alev Erisir

^aDepartment of Chemical Engineering, University of Virginia, Charlottesville, Virginia 22904, USA; ^bDepartment of Psychology, University of Virginia, Charlottesville, Virginia 22904, USA; ^cSchool of Materials Science and Engineering, Gwangju Institute of Science and Technology (GIST), Gwangju 61005, Republic of Korea

Abstract: Reducing amyloid- β (A β) accumulation is a promising strategy for developing Alzheimer's Disease (AD) therapeutics. We recently reported that a triphenylmethane food dye analog, Brilliant Blue G (BBG), is a dose-dependent modulator of *in vitro* amyloid- β aggregation and cytotoxicity in cell-based assays. Following up on

this recent work, we sought to further evaluate this novel modulator in a therapeutically-relevant AD transgenic mouse model. BBG was orally administered to APPSwDI/NOS2^{-/-} mice for three months in order to assess its biocompatibility, its permeability across the blood-brain barrier, and its efficacy at rescuing AD pathology. The results showed that BBG was well-tolerated, caused no significant weight change/unusual behavior, and was able to significantly cross the AD blood-brain barrier in APPSwDI/NOS2^{-/-} mice. Immunohistochemical and electron microscopic analysis of the brain sections revealed that BBG was able to significantly prevent neuronal loss and reduce intracellular APP/A β in hippocampal neurons. This is the first report of 1) the effect of Brilliant Blue G on neuronal loss in a transgenic animal model of AD, 2) oral administration of BBG to affect a protein conformation/aggregation disease, and 3) electron microscopic ultrastructural analysis of AD pathology in APPSwDI/NOS2^{-/-} mice.



Inchan Kwon

Keywords: Alzheimer's Disease, amyloid- β , blood-brain barrier, intracellular amyloid- β , neuronal loss, triphenylmethane dye.

INTRODUCTION

Alzheimer's Disease (AD), the most common form of senile dementia, is characterized and diagnosed by three key pathological hallmarks: neurofibrillary tau protein tangles, neuronal loss, and the accumulation of insoluble peptide aggregates, composed primarily of neurotoxic amyloid- β (A β) [1, 2]. The amyloid-cascade hypothesis states that A β accumulation is toxic to the brain and causative to the tau pathologies leading to neuronal death and cognitive deficits seen in AD patients [3, 4]. Therefore, reducing A β accumulation can be a promising strategy in developing AD therapeutics.

Numerous small molecules have been studied for their ability to modulate A β aggregation and reduce neurotoxicity [5, 6]. Although the results from these studies are encouraging in validating A β aggregation modulation as a promising strategy, a practical, safe, and effective agent has yet to be identified. In order to search for novel small molecule modulators with good biocompatibility, our research group screened various FDA-approved food dyes and their close

structural analogs. We recently reported that the triphenylmethane food dye analog, Brilliant Blue G (BBG), which is a P2X7 receptor antagonist, is a novel modulator of *in vitro* A β 40-aggregation and A β cytotoxicity in cell-based assays [7, 8]. Following up on this recent work, we sought to further evaluate BBG's efficacy *in vivo*, in a therapeutically-relevant AD transgenic mouse model.

The *in vivo* efficacy of intravenously (IV) or intraperitoneally (IP) injected BBG against neurodegenerative protein conformation/aggregation diseases has been widely investigated [9-15]. In a non-transgenic AD model that simulated the inflammation state of the disease via soluble hippocampal A β 42 injections, intraperitoneal injections of BBG resulted in an increase of the viable neurons, a reduction in gliosis/inflammatory response, and a decrease in blood-brain barrier leakage [16], as well as improved cognitive function [17]. The effect of BBG on A β pathology in a transgenic mouse model of familial AD was first assessed in 2012 [18]; intraperitoneal injection of the compound to J20 hAPP mice revealed that BBG effectively penetrated the brain-blood barrier (BBB) and reduced the number and size of A β plaques in hippocampus. Whether BBG also prevents neuronal loss, an important characterization step in the development of BBG as a lead AD therapeutic candidate, remained unknown [18]. Our current study aimed to provide the evidence that BBG can prevent neuronal loss, using a transgenic model of AD that displays substantial cell loss.

*Address correspondence to these authors at the 102 Gilmer Hall, PO Box 400400, Department of Psychology, University of Virginia, Charlottesville, Virginia 22904, USA erisir@virginia.edu, and School of Materials Science and Engineering, Gwangju Institute of Science and Technology, 123 Cheomdan-gwagiro, Buk-gu, Gwangju 61005, Republic of Korea; Tel: 82-62-715-2312; E-mail: inchan@gist.ac.kr

We used a previously well-established mouse model, APPSwDI/NOS2^{-/-}, to investigate the effect of oral administration of BBG on neuronal loss and also APP/A β staining. The APPSwDI/NOS2^{-/-} transgenic strain was generated by crossing the widely accepted cerebral amyloidosis angiopathic model APPSwDI (Amyloid- β Protein Precursor with Swedish K670N/M671L, Dutch E693Q, and Iowa D694N mutations) transgenic mice with NOS2^{-/-} (nitric oxide synthase 2 encoding gene knockout) mice [19-21]. NOS2 expression has been reported as having differing effects in AD in transgenic models. On one hand, NOS2 expression has been shown to play a neuroprotective role. Furthermore, since macrophages in the mouse brain display more activity in producing nitric oxide that provides protection during an immune response than human macrophages, knocking out the NOS2 gene allows for a better representation of human brain pathology in a mouse model [3, 22]. Conversely, in certain transgenic mouse models, NOS2 expression exacerbates AD pathology, and NOS2 genetic deletion can in fact be neuroprotective [23, 24]. Regardless of the mode of action of NOS2, APPSwDI/NOS2^{-/-} transgenic model of AD has been validated as displaying all cardinal signs of AD, that is, severe amyloid deposition, tau pathology, 30-40% hippocampal neuron loss, and significant memory deficits revealed at the radial-arm water maze by 12-14 months of age [3, 19-21, 25, 26], and thus constitutes an excellent model to assess the potency of BBG on rescuing cell death in AD. The results of our current study provide the first report of the effect of BBG on neuronal loss in a transgenic animal model of AD, as well as the first report of oral (not IV or IP) administration of BBG, which affected a protein conformation/aggregation disease.

MATERIALS AND METHODS

Mice

Female 6-7 month old wild type C57BL/6 (Jackson Laboratories) and APPSwDI/NOS2^{-/-} familial AD transgenic mice, derived from female C57BL/6 mice, were used. A total of 10 - WT and 8 - APPSwDI/NOS2^{-/-} transgenic mice were randomly divided up into untreated control and drug experimental, WT and transgenic groups. This resulted in the following treatment group compositions: WT untreated control = 5 mice, WT drug experimental = 5 mice, APPSwDI/NOS2^{-/-} untreated control = 4 mice, APPSwDI/NOS2^{-/-} drug experimental = 4 mice. All procedures using vertebrate animals were approved by the University of Virginia Institutional Animal Care and Use Committee (IACUC).

BBG Preparation, Administration and Monitoring

BBG was prepared by blending dry powder of the compound (Sigma Aldrich, \geq 95% purity) into standard mice chow; the mixture containing 2,000 mg/kg/day BBG was provided ad libitum for 3 months. The oral dose was determined based on previously reported safe dosages for oral and injected BBG [27, 28] and assuming 5% absorption by the gastro-intestinal tract following oral consumption based on studies with Brilliant Blue FCF (BBF – FDA approved food dye, FD&C blue No. 1, since detailed metabolic loss studies have not been conducted with BBG), a close structural ana-

log of BBG [29]. Mice in the untreated control groups were fed standard basal mouse chow diet. The period of treatment (3 months) is comparable to previous studies that tested the efficacy of drug candidates on A β in mouse AD-models (ranging from 2 weeks to 6 months) [30-35].

To assess gross biocompatibility, biodistribution and any potential gross toxic effects, the coloring of extremities, the urine and the feces, the appearance of skin, haircoat, eyes and the posture, unusual behaviors and signs of distress were observed 1-2 times per week throughout the BBG treatment period. The weight of each mouse was measured weekly.

Tissue Processing for Neuroanatomical and Biochemical Analysis

At the end of the 3-month BBG-administration regimen, mice (which reached 9-10 months of age by that time) were given an overdose of Euthasol solution (IP), followed by transcatheter aldehyde perfusion. For neuroanatomical analysis, 3 mice per treatment group were perfused transcatheterially with Tyrode's buffer followed by a mixture of 4% paraformaldehyde and 0.1% glutaraldehyde. Extracted brains were post-fixed overnight at 4°C in the same fixatives, cut in to 60 μ m thick coronal sections on a vibratome (Leica VT1000S), collected serially in a 12-well plate, and then they were treated with 1% NaBH₄ for 30 minutes to deactivate fixative. For biochemical BBG tissue concentration analysis, 1-2 mice per treatment group were perfused transcatheterially with PBS only. Following extraction from the skull and parasagittal bisection, the hemibrains were flash-frozen in liquid nitrogen and subsequently stored at -70°C.

Tissue Preparation for Electron Microscopy

Vibratome-sectioned sections were counterstained, resin-embedded, and ultrathin sectioned using routine protocols [36-38]. The sections were incubated in 1% osmium tetroxide in PB for 1 hour, and in 4% uranyl acetate dissolved in 70% ethanol for 2-18 hours. The sections were then dehydrated sequentially in increasing concentrations of ethanol and acetone (EM grade, EMS). Sections were then treated with 50/50 acetone/resin (EMBED812; EMS) mixture for 2 hours, then with 100% resin overnight. Sections were placed between two acetate sheets, and cured in a 60°C oven for 1-2 days. These flat-embedded sections were examined with a light microscope to identify tissue landmarks for the region of interest in hippocampus, which was consequently excised and re-polymerized at the bottom of BEEM capsules. The features of capsule-embedded sections were sketched in detail, and the block was trimmed to a 2x1mm trapezoidal block that spanned the hippocampus CA1 pyramidal and striatum radiatum layers dorso-ventrally. Ultrathin sections (70-90nm) were cut using a Leica Ultracut UCT and collected on 200-mesh nickel grids.

Quantification of BBG in Brain Tissue

The extent of BBG diffusion across the blood-brain barrier was assessed by spectroscopic absorbance measurements of the blue dye concentration in snap-frozen tissue [39]. After the flash-frozen brain tissue was thawed, the wet weight and volume of each hemisphere was measured. Next, 5 mL

of 1X PBS (10 mM NaH₂PO₄ and 150 mM NaCl, pH 7.4) was added to each brain in a 15 mL centrifuge tube, placed on ice, and the tissue was homogenized with an ultrasonic converter (Branson Sonifier model 102C CE equipped with a Fisher Scientific Sonic Dismembrator Model 500 Control System, 30 minutes, 10% amplitude, 15 seconds on pulse, 5 seconds off pulse). Samples of the brain homogenate (100 μ L samples; $n \geq 20$ replicates for 1-2 mice per group) were aliquoted into a 96-well plate. Next, the absorbance spectra were scanned from 200-800 nm with a Synergy 4 UV-Vis/fluorescence multi-mode microplate reader (Biotek), reading the maximal absorbance of BBG at 576 nm, and using 800 nm as a reference point to correct for tissue sample differences. The average BBG concentration (\pm SEM) in the tissue of experimental groups was quantified via correlation to calibration curves constructed by adding known amounts of BBG to homogenized brain tissue from untreated control mice that did not receive the dye compound.

Immunohistochemistry

Non-specific IgG binding was blocked by treating brain sections with 1% BSA, 0.01M PBS solution for 30 minutes at room temperature. Sections were then incubated with one of the following primary antibodies prepared in PBS containing 1% BSA and 0.05% NaN₃ (to prevent bacterial growth) overnight at room temperature: monoclonal anti-6E10 (1:200; Covance, Catalog #: SIG-39320), which recognizes the N-terminal 4-9 amino acid residues of A β [32, 40], and monoclonal anti-NeuN (1:200; Millipore, Catalog #: MAB377), a widely characterized antibody that recognizes a neuronal-specific nuclear protein [3, 41]. The brain sections were then treated in biotinylated anti-mouse secondary antibody (Vector Labs, Catalog #: BA-9200; 1:1000 and 1:100 dilutions were used for 6E10 and NeuN, respectively) for 2 hours at room temperature, followed by incubation in avidin-biotin complex (Vectastain ABC Elite Kit; Vector Labs). The antibody binding was visualized with 3,3'-diaminobenzidine, tetrahydrochloride (DAB) reaction. Finally, the sections were mounted on subbed slides, air-dried, dehydrated with ethanol, de-fatted with xylene, and cover-slipped using DPX mountant.

Imaging

The patterns of immunohistochemical stain were imaged using a light microscope (Zeiss Axio Imager M2 with motorized z-scan equipped with a Zeiss AxioCam Ice3 digital camera). To ensure comparable brain sections were analyzed from each animal, sections that contain dorsal hippocampus were selected for analysis. The AP coordinates of the sections were comparable to Allen Mouse Brain Reference Atlas, coronal images 70-76 (<http://mouse.brain-map.org/static/atlas>) for hippocampus analysis, 80-89 for subiculum analysis, and 70-89 for cortex analysis. For 6E10, images from the CA1-CA2 regions of hippocampus and from the cerebral cortex were captured for each brain section (1-4 sections per animal) using the 20x objective lens, yielding 0.9 mm² (CA1-CA2) and 1.1 mm² (cortex) total tissue area per section. For NeuN, images from the CA1 and subiculum hippocampal regions were captured for each brain section (2-5 sections per animal, \sim 5.6 mm² total area per

section) using the 10x objective lens on a Leica DMLB light microscope equipped with a Leica MC170 HD digital camera. Ultrathin sections were examined on a JEOL 1010 transmission electron microscope. Images of ultrastructural pathology were captured using a 16M pixel digital camera (SIA-12C, Scientific Instruments and Applications, Duluth, GA) at 10000x or 15000x magnifications.

Quantification of Neuronal Loss and APP/A β Accumulation

While stereological approaches, such as bisector method, are most suitable to obtain unbiased counts of neurons in identified brain regions, areal neuron density measurements are reliably used to quantify neuronal loss in neurodegenerative models [42-45]. In the current study, neuronal loss in hippocampus was assessed by non-blinded quantification of areal density of NeuN labeled cells, and the measurements of the thickness of pyramidal cell layer, using Image J software (NIH). To assess areal neuron density in subiculum, a stereology grid with 70x70 μ m grid-boxes was placed on the cell layer, using Grid and Cell Counter plugins in Image J (Supplementary Fig. S1B). While 35-40 grid-boxes typically covered subiculum in the WT cases, only the grid boxes that remained fully within the subiculum borders were analyzed. The cells within the grid-square were counted manually following stereology principles, and the average density of neurons in each grid-box was calculated for each brain. Areal density measures were quantified in 1-3 sections per brain, 3 brains/mice per condition, across 4 total conditions (treatment groups). This quantification yielded areal density measures from ≥ 350 counting grid squares per condition. A similar analysis was initially run for CA1 and CA2 regions of the hippocampus, where pyramidal cell layer contained tightly packed cell bodies in a narrow layer. Because a cell loss in this region leads to a collapse in the thickness of the cell layer, rendering cell density measures unreliable, we used the cell layer thickness as a proxy for the number of neurons. The thickness of the CA1-CA2 pyramidal cell layer was measured along a line that was perpendicular to pial surface and the white matter (Supplementary Fig. S1A). Multiple measurements that were 70 μ m apart at the pial surface were taken from each CA1-CA2 image.

APP/A β accumulation in the brain tissue was quantified through non-blinded assessment of the percentage of 6E10 labeled area per total area examined. On images containing 6E10 labeled hippocampus, the background pixel intensity was measured from the unstained neuropil directly dorsal to the CA1-CA2 pyramidal cell layer of each section. The 6E10 labeled regions were then identified as label intensity higher than 4X the background intensity in the same sections (Image Pro Plus 7.0, Mediacy). The percent ratio of 6E10 positive areas was computed within the grid squares placed on pyramidal cell layer. In each section 40-167 (depending on number of grid squares fully remained within the cell layer) grid-squares were analyzed. In cerebral cortex sections, where, in contrast to hippocampus, the neuronal somata are sparsely distributed, APP/A β accumulation was assessed by manually tracing the area (in Image J) occupied by diffuse plaques stained by the 6E10 antibody within randomly placed grid-squares, excluding labeled cells. As a result, the APP/A β accumulation analysis in cerebral cortex

reflects localization in the neuropil regions rather than in the cell bodies.

The within variable averages of NeuN and 6E10 staining analyses were compared between transgenic, wild type, and untreated control animal groups using one-way ANOVA ($p < 0.05$ required for significance) followed by Tukey's post-hoc analysis to determine significant differences.

RESULTS

Administration of BBG is Well-Tolerated, Achieves Peripheral Biodistribution, and Effectively Penetrates the BBB in AD Transgenic Mice

The oral administration of BBG for three months was well-tolerated: Animals did not show any overt aversive behavior toward BBG blended chow, indicating BBG did not change the palatability of the food. Observations during the administration period revealed no signs of malnutrition or toxicity. Weekly body weight measurements revealed that untreated control wild type mice (WT Control) gained significantly more weight than the untreated control APP-SwDI/NOS2^{-/-} (APP Control) group ($p = 0.02$, one-way ANOVA + Tukey's post-hoc analysis, $n = 14$ data points of each group's change in average weight in a respective week during the 3 month BBG administration period compared to starting weight; Table 1, Fig. 1), suggesting strain differences play a role in body weight change and eating habits. However, oral administration of BBG was not found to significantly affect overall average weight change in either mouse strain ($p = 0.4$; Fig. 1), although it did cause an increase in week-to-week fluctuation of the weights of individual APPSwDI/NOS2^{-/-} mice ($p = 0.00001$ in comparing SEMs of APP Cont. and BBG groups, as shown in Table 1, $n = 14$).

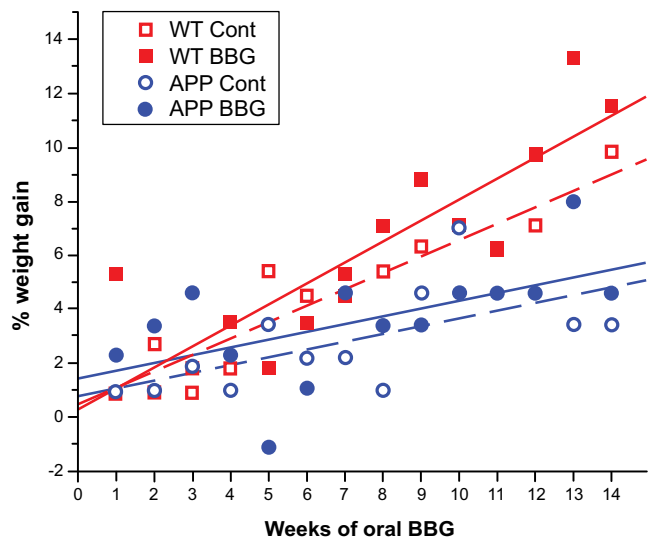


Fig. (1). Percent weight change in APPSwDI/NOS2^{-/-} (APP; circles) and wild type (WT; squares) mice with (filled markers) or without (unfilled markers) oral administration of BBG. Each data point is the percent change in particular group's average weight relative to the starting weight at a given week during the 3 month BBG administration period ($n = 4-5$ mice per group). Dashed and solid functions are linear regression lines for untreated and BBG treated groups, respectively.

To assess the biodistribution and bioavailability of BBG (a blue-colored dye) upon administration, the animals were observed 1-2 times per week for presence of blue coloring at their body parts, urine, and feces. Starting approximately 4 days after beginning the BBG administration period, mice in both the WT type and APP groups displayed a light bluish-green hue on the extremities (nose, ears, skin) as well as a darker blue color in the urine and fecal matter, indicating that the compound was absorbed, peripherally distributed, and excreted.

To assess whether BBG crosses the blood-brain barrier, the concentration of the blue dye in homogenized brain tissue was quantified at the end of the 3 months oral BBG administration period, using a spectrophotometer at the maximal absorbance of BBG at 576 nm. Reference-subtracted absorbance measurements (800nm was used for reference absorbance) normalized to untreated controls revealed no significant difference between WT Control (1.00 ± 0.03) and WT BBG (1.04 ± 0.01) groups ($p = 0.09$ from one-way ANOVA test, $n \geq 20$ replicate measurements) in wild type mice, indicating that the compound was not able to significantly pass through the BBB of healthy brains. Most exogenous molecules, such as BBG, that passively cross the BBB through endothelial transcellular diffusion are lipophilic and less than 450 Da in size [46, 47]. In contrast, BBG is water-soluble and has a molecular weight over 800 Da [48], making passive diffusion of this compound across BBB unlikely. The most likely BBB-permeation mechanism for BBG is the paracellular passages between endothelial cells, that is, extremely robust tight junctions sealed with protein complexes [49]. Thus, the passage of BBG through the healthy, intact BBB of a mouse is unlikely, and this was confirmed by our wild type mice results.

However, in the transgenic APPSwDI/NOS2^{-/-} familial AD mice fed with BBG (APP BBG group), reference-subtracted normalized spectrophotometric absorbance at 576 nm (1.26 ± 0.01) was significantly ($p = 1.33 \times 10^{-31}$, one-way ANOVA + Tukey's post-hoc analysis, $n \geq 20$ replicate measurements in each case) higher than in the untreated APPSwDI/NOS2^{-/-} (APP Cont., 1.00 ± 0.01) group. The BBG concentration in the brain tissue was $3.91 \pm 0.13 \mu\text{M}$ in BBG treated AD animals, suggesting that conditions that rendered transgenic mice unhealthy also compromised the BBB for BBG passage.

BBG Prevents Hippocampal Neuronal Loss in AD Model

Given that it is an important AD-associated pathological feature and there have been no prior reports characterizing the effect in a transgenic animal model of AD, we next investigated whether oral administration of BBG could alleviate the loss of neurons that occurs in transgenic familial AD mouse model. To this aim, we visualized neuronal cell bodies using NeuN immunocytochemistry. The quantifications of neuron areal density in the subiculum and the thickness of pyramidal cell layer in CA1-CA2 revealed no significant differences ($p = 0.2$ and 0.1 for subiculum and CA1-CA2, respectively, from one-way ANOVA test) between untreated WT and BBG fed WT animals (Fig. 2A-C, Fig. 3A-C, and Table 2A-B). Combined with the finding that BBG permeability to WT brains is negligible, the absence of

Table 1. Weekly weight monitoring during 3 month oral Brilliant Blue G (BBG) administration period. Percent weight change of APPSwDI/NOS2^{-/-} (APP) and wild type (WT) untreated (Cont.) and orally-administered BBG (BBG-Food) mice. Data expressed as the overall change in each group's average weight in a respective week during 3 month BBG administration period compared to starting weight, +/- SEM (n = 4-5 mice per group).

Group	% Weight Change During 3 Month BBG Administration Period Compared To Starting Weight													
	1	2	3	4	5	6	7	8	9	10	11	12	13	14
WT Cont.	0.9 ± 1.1%	2.7 ± 2.0%	0.9 ± 1.1%	1.8 ± 0.9%	5.4 ± 1.1%	4.5 ± 1.8%	4.5 ± 2.3%	5.4 ± 1.1%	6.3 ± 1.7%	7.1 ± 2.4%	6.3 ± 1.7%	7.1 ± 2.4%	8.0 ± 2.2%	9.8 ± 2.3%
WT BBG-Food	5.3 ± 1.7%	0.9 ± 1.7%	1.8 ± 1.4%	3.5 ± 2.3%	1.8 ± 1.4%	3.5 ± 1.1%	5.3 ± 1.7%	7.1 ± 1.7%	8.8 ± 3.0%	7.1 ± 1.7%	6.2 ± 1.4%	9.7 ± 2.2%	13.3 ± 3.0%	11.5 ± 2.2%
APP Cont.	1.0 ± 1.5%	1.0 ± 2.2%	1.9 ± 1.0%	1.0 ± 0.0%	3.4 ± 1.4%	2.2 ± 1.2%	2.2 ± 1.2%	1.0 ± 2.0%	4.6 ± 2.3%	7.0 ± 2.3%	4.6 ± 1.2%	4.6 ± 1.2%	3.4 ± 1.4%	3.4 ± 1.4%
APP BBG-Food	2.3 ± 3.4%	3.4 ± 3.0%	4.6 ± 2.9%	2.3 ± 2.9%	-1.1 ± 1.3%	1.1 ± 1.9%	4.6 ± 2.2%	3.4 ± 3.0%	3.4 ± 3.0%	4.6 ± 2.2%	4.6 ± 3.4%	4.6 ± 3.4%	8.0 ± 3.0%	4.6 ± 2.2%

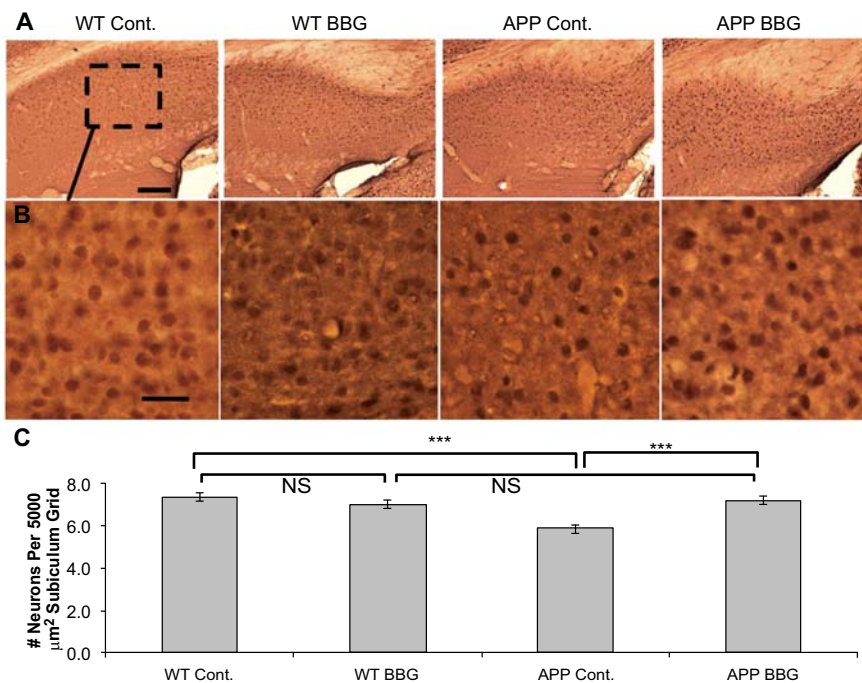


Fig. (2). NeuN immunohistochemical assessment of neuronal loss in subiculum field of hippocampus with oral BBG administration. **A, B** Light microscopy images of NeuN staining in the subiculum field of the hippocampus for wild type (WT) and APPSwDI/NOS2^{-/-} (APP) mice either untreated (-Cont. groups) or orally administered BBG for 3 months (-BBG groups). Scale bar in **A** = 150 μm; scale bar in **B** = 50 μm. **C.** Neuron areal density was computed as the number of neurons within a counting square placed in the subiculum (also see Supplementary Fig. S1). Data expressed as average ± SEM (n ≥ 350 total counting squares from 3 animals per group). *** indicates significant difference (p < 0.0001 from one-way ANOVA + Tukey post-hoc analysis). NS indicates no significant difference detected (p > 0.1).

pyramidal cell differences after BBG administration in WT animals suggests that oral BBG does not have any, neither detrimental nor proliferative, effect on hippocampal cell health. In contrast, compared to WT Control animals, the APP Control animals displayed 20-22% neuronal loss both in the subiculum and in the CA1-CA2 region (p = 1.7 × 10⁻⁸ and 5.8 × 10⁻²⁶ from one-way ANOVA + Tukey's post-hoc analysis for subiculum and CA1-CA2, respectively, Fig. 2

and Fig. 3, and Table 2A-B). A previous study that validated the APPSwDI/NOS2^{-/-} transgenic AD mouse model revealed 35-40% neuron loss in the subiculum and the CA regions of the hippocampus of 12-14 months old mice (3). In our study, 9-10 months old APPSwDI/NOS2^{-/-} mice displayed 20-22% neuronal loss in these same regions. Since AD-related neurodegeneration increases with age [50], we postulate that the comparatively less (but still highly signifi-

Table 2. NeuN neuronal loss quantification. Numerical/tabular presentation of the *A*, number of neurons counted per 5000 μm^2 subiculum grid and of the *B*, average measured thickness of the CA1-CA2 pyramidal neuron cell layer displayed graphically in Fig. 1C and Fig. 2C, respectively. Data expressed as average \pm SEM. Right column displays the number of individual measurements assessed to obtain the displayed average.

A.

Treatment Group	Average # Neurons Per 5000 μm^2 Subiculum Grid \pm SEM	# of Measurements
WT Cont.	7.3 \pm 0.2	350
WT BBG-Food	7.0 \pm 0.2	403
APP Cont.	5.9 \pm 0.2	361
APP BBG-Food	7.2 \pm 0.2	395

B.

Treatment Group	Average CA1-2 Neuronal Layer Thickness (μm) \pm SEM	# of Measurements
WT Cont.	74 \pm 1	463
WT BBG-Food	77 \pm 2	500
APP Cont.	58 \pm 1	413
APP BBG-Food	76 \pm 2	420

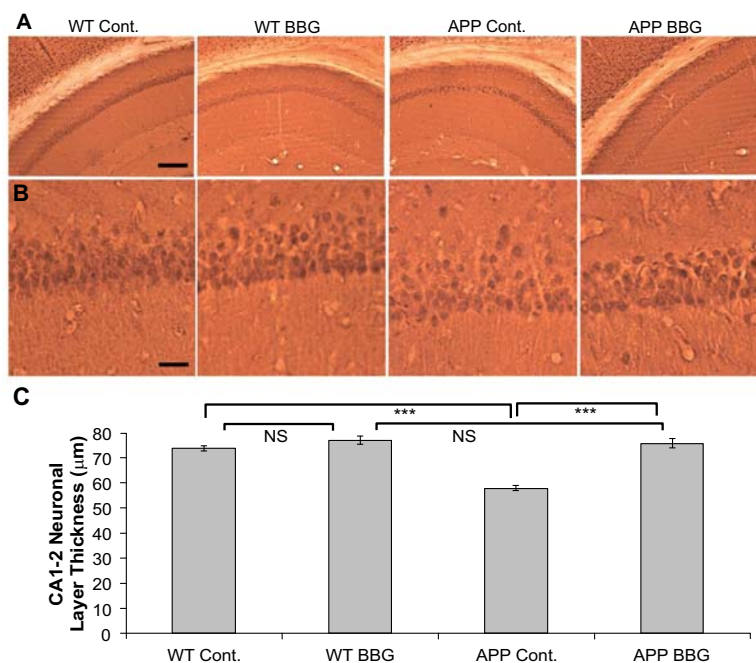


Fig. (3). NeuN immunohistochemical assessment of neuronal loss in CA1-CA2 neuronal cell layer of hippocampus with oral Brilliant Blue G (BBG) administration. **A,B** Representative light microscopy images of NeuN staining in the CA1-CA2 cell layer of the hippocampus for wild type (WT) and APPSwDI/NOS2^{-/-} (APP) mice either untreated (APP Cont.) or orally administered BBG for 3 months (APP BBG). Scale bar = 160 μm for the **A**, and 40 μm for **B** panels, zoomed in view of the CA1-2 neuronal cell layer measured. Note that the close packing of pyramidal cells in hippocampus reduces the reliability for identifying individual cells. Furthermore, loss of cells in APP-Cont cases disrupts cell-packing density in this region, precluding areal cell-density measures. **C**, Neuronal loss was quantified by measuring width/thickness of the CA1-2 neuron layer (also see Supplementary Fig. S1A). Data expressed as average \pm SEM ($n \geq 400$ replicates, 3 animals per group). *** indicates significant difference ($p < 0.0001$ from one-way ANOVA + Tukey's post-hoc analysis). NS indicates no significant difference detected ($p > 0.05$).

cant) neuronal loss observed in our tissue was due to assessing mice at a younger age.

The administration of BBG prevented this neuronal loss. The neuron density and pyramidal cell layer thickness in APP BBG brains was higher than that in APP Control group ($p = 3.9 \times 10^{-8}$ and 3.0×10^{-17} from one-way ANOVA + Tukey's post-hoc analysis for subiculum and CA1-CA2, respectively, Fig. 2, Fig. 3, and Table 2), while no statistically significant differences existed between APP BBG and WT BBG mice ($p = 0.4$ and 0.6 for subiculum and CA1-CA2, respectively, Fig. 2, Fig. 3, and Table 2). This suggests that oral administration of BBG for 3 months has prevented the neuronal loss that occurs in the hippocampus of APP-SwDI/NOS2^{-/-} mice.

BBG Reduces Intracellular APP/A β Staining in the CA1-CA2 Pyramidal Cell Layer of the Hippocampus, But Does not Affect the Plaques in Cerebral Cortex Neuropil

In order to assess whether oral BBG administration also prevented the amyloid pathology, the 6E10 primary antibody was used to analyze the extent of staining in the CA1-CA2 pyramidal cell layer of the hippocampus. As reported before, the majority of 6E10 staining in CA pyramidal cell layer was localized on neuronal bodies (Fig. 4, [51-55]). The CA pyramidal cell layer is densely packed with neurons, and therefore, the area analyzed here was almost completely composed of somata. In the literature, some discord exists regarding the exact APP and/or APP-cleavage product and aggregation-state of intracellular A β staining seen in transgenic mice models and human AD patients when using sequence-specific antibodies, such as 6E10 [56-59]. A substantial body of literature indicates that intracellular staining by these sequence-specific antibodies does indeed represent primarily the aggregation prone A β 42 but not Amyloid- β Protein Precursor (APP) parent protein or other cleavage product [55, 60, 61]. It should also be noted that in transgenic models based on overexpression of human APP gene, the majority of 6E10 staining is expected to be overexpressed human protein, rather than mice APP [62]. Aggregated A β species can also be identified using oligomer-specific antibodies or less specific histochemical methods, such as Thioflavin S [63-70]. We rather chose to use the pan-amyloid 6E10 antibody to capture all forms of APP and A β expressed in this mice model. Although we cannot be sure that 6E10 staining is a reliable indicator of the amount of intracellular A β , nor a marker for extracellular amyloidosis, we used this antibody as a generic marker for amyloid pathology (APP/A β) that develops in hippocampal cells of this transgenic model.

In wild type mice, only ~ 0.1% of the CA neuron layer was labeled with 6E10, indicating negligible APP/A β accumulation (Fig. 4 and Table 3A). In APP Control brains, 6E10 stain occupied ~ 10% of the total area, which was 100 times more than in the WT Control brains (Fig. 4 and Table 3A), indicating negligible false-positive interfering background signal resulting from sources such as endogenous mouse antibodies. It is conceivable that this staining represents de novo APP transcript in this transgenic model, as well as intracellular A β . In contrast to APP Cont brains, in the APP BBG group, only about 5% of the area analyzed was occu-

ried by 6E10 positive stain, indicating a significant ($p = 4.0 \times 10^{-24}$, one-way ANOVA + Tukey's post-hoc analysis) difference in APP/A β accumulation in comparison to APP Control (Fig. 4E and Table 3A). Because we cannot postulate any BBG effect in slowing down APP transcription in these neurons, we propose that the reduction in 6E10 staining in APP BBG animals represents a slow-down of toxic A β accumulation in AD mice. Concurrent reduction of cell death in BBG treated APP animals, as demonstrated in the current study, also supports the idea that BBG treatment reduces A β toxicity, rather than APP transcription.

In the cerebral cortex of both the control and BBG-fed APPSwDI/NOS2^{-/-} animals, 6E10 immunoreactivity was observed in or around both the neuronal cell bodies and the neuropil (that is, the brain volume occupied by components other than somata), appearing as varying sizes of labeled patches (Fig. 5A-B). We assessed the extent of these diffuse, neuropil plaques by tracing the borders of each plaque in Image J, and calculating the ratio of areas occupied by 6E10 positive plaques in each section. There was no significant difference in the percentage of area occupied by the plaques between APP Control and APP BBG mice ($p = 0.7$ from one-way ANOVA test, Fig. 5C and Table 3B). In addition, oral administration of BBG did not significantly affect the average area of individual plaques traced; the average plaque sizes in APP Control and APP BBG mice were $626 \pm 24 \mu\text{m}^2$ and $678 \pm 26 \mu\text{m}^2$, respectively ($p = 0.2$ from one-way ANOVA test, $n > 600$ individual plaque area measurements). This finding implies different mechanisms for formation of amyloid plaques and the APP/A β -dependent neuropathology that leads to cell death in this transgenic APP mice model. The 6E10 label was also observed as varying sizes of patches in striatum radiatum, the cell-sparse layer containing apical dendrites of pyramidal cells, and in dentate gyrus, however A β accumulation in these regions was not quantified further.

EM Demonstration that BBG Reduces Neuron Degeneration in Hippocampus

In order to assess ultrastructural properties of mice hippocampal pathology encountered in APP Control and APP BBG mice, we examined ultrathin sections from hippocampus of animals in each group using electron microscopy. Both brains displayed hallmark ultrastructural pathology of AD brains, including amyloid plaques, myelinated bulbs, autophagosomic formations and vacuoles, multilamellar bodies, dystrophic neurites, bundled filaments and lipofuscin bodies (Supplementary Fig. S2, Fig. 6A, C-F) [71-73]. The most notable qualitative difference in neuropathological formations observed between APP Control and APP BBG brains was the lack of degenerating cell bodies in CA1: In the pyramidal cell layer of APP Control animal hippocampus, the normal cellular arrangement was disrupted by degenerating somata and autophagosomic formations (Fig. 6A vs. B). Degenerating neurites, which often were filled with massive bundles of filaments (Fig. 6D and 6G), were observed. It is interesting that fibrillar accumulations in pyramidal cells and dendrites (e.g., Fig. 6D, G) were distinct from electron dense, vacuous and multilamellar degeneration products (e.g., Fig. 6A-B) observed in pyramidal cell layer of untreated mice brains (APP Cont), possibly indicating either two distinct stages or types (i.e., amyloid and tau) of

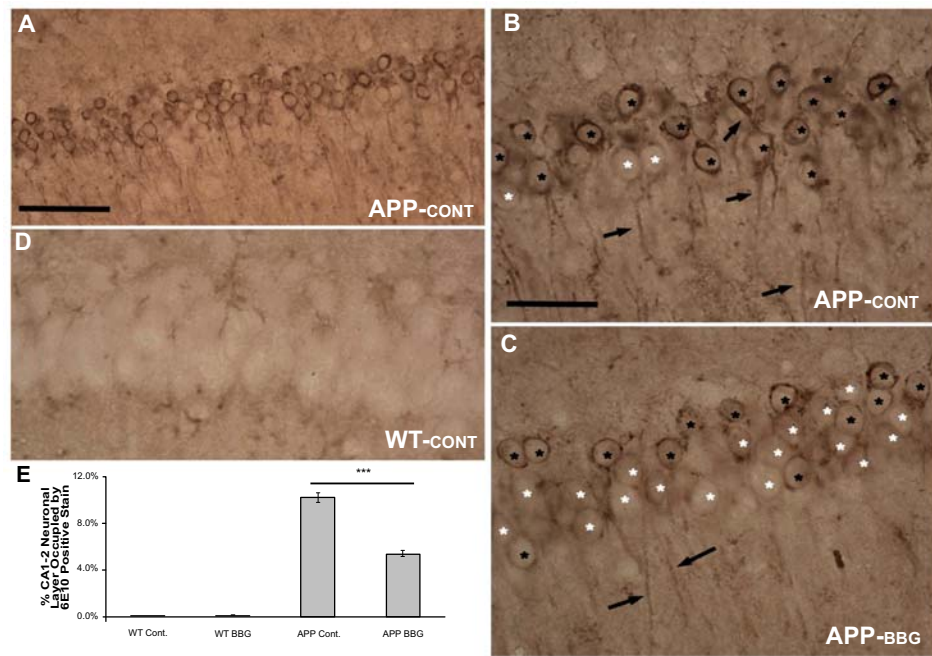


Fig. (4). 6E10 staining in CA1 pyramidal cell layer of hippocampus, in WT and APP transgenic mice with oral Brilliant Blue G (BBG) administration. *A-C*. Treatment with 6E10 antibody leads to visualization of dark accumulation in APP mice hippocampus neurons (black asterisks), while some unstained cells remain discernable (white asterisk). Compared to BBG fed mice (*C*), a larger number of cells were stained in APP-Cont mice (untreated group, *A-B*). The cells in APP-Cont brains were less organized, and they were dysmorphic, displaying wider spaces between discernable somata. The 6E10 staining was negligible in WT brains with or without (*D*) BBG treatment. Scale bar in *A*= 100 μm. Scale bar in *B*= 50 μm and applies for panels *B-D*. *E*, Quantification of intracellular Aβ staining in neurons expressed as the average percentage of area occupied by 6E10-positive stain per total area analyzed ± SEM (n ≥ 450 measurement squares, 2-3 animals per group). *** = p < 0.0001 (one-way ANOVA + Tukey’s post-hoc analysis).

Table 3. 6E10 Aβ staining quantification. Numerical/tabular presentation of *A*, the percent area of the CA1-CA2 pyramidal neuron cell layer occupied by 6E10-positive stain, and of *B*, the percent area of cortex neuropil occupied by 6E10-positive diffuse plaques displayed graphically in Fig. 3C and Fig. 4C, respectively. Data expressed as average ± SEM. Right column displays the total number of measurements obtained from 3 animals in each group.

A.

Treatment Group	Average % CA1-2 Neuronal Layer Area Occupied by 6E10 Positive Stain ± SEM	# of Measurements
WT Cont.	0.08 ± 0.03	145
WT BBG-Food	0.11 ± 0.03	215
APP Cont.	10.21 ± 0.39	456
APP BBG-Food	5.43 ± 0.27	662

B.

Treatment Group	Average % Cortex Neuropil Area Occupied by 6E10 Positive Diffuse Plaques ± SEM	# of Measurements
WT Cont.	1.1 ± 0.2	30
WT BBG-Food	0.8 ± 0.2	25
APP Cont.	9.1 ± 0.9	50
APP BBG-Food	8.6 ± 0.7	83

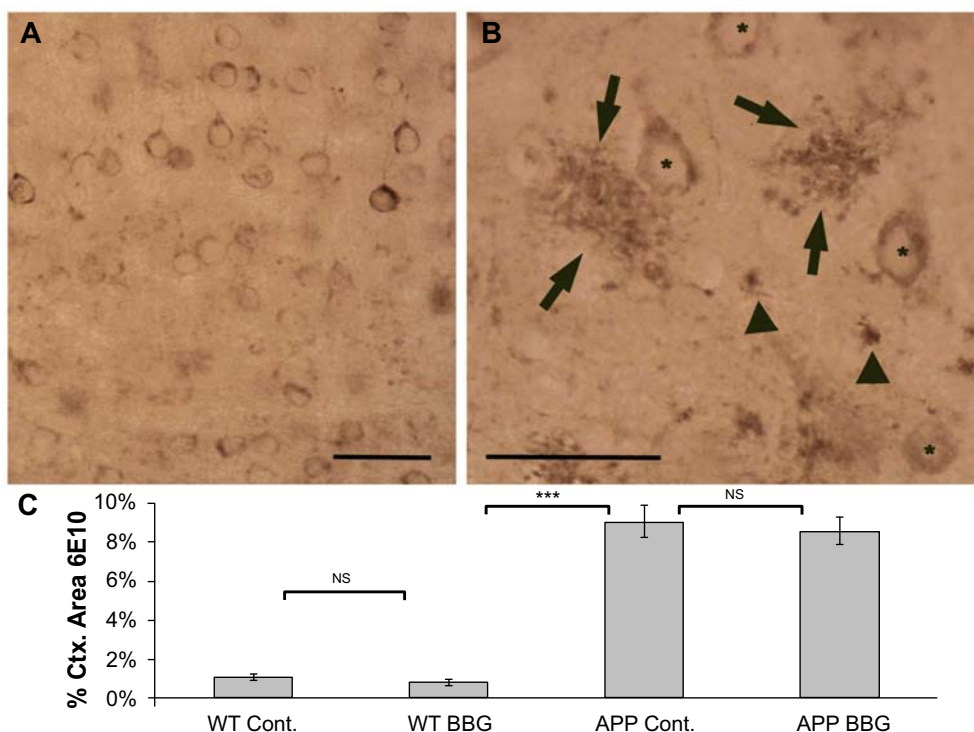


Fig. (5). Immunohistochemical assessment of 6E10 staining in the cortex neuropil with oral Brilliant Blue G (BBG) administration. **A,B** The 6E10 immunoreaction lead to visualization of neurons (black asterisk) in all layers of the cerebral cortex (Ctx.) in APP mice. Extracellular accumulation of 6E10 stained product was also prevalent throughout cortex (**B**), as well as in dentate gyrus (not shown). The size of these amyloid accumulations (plaques) ranged from punctate (arrowheads) to 80-100 μm (black arrows), leading to a diffuse staining appearance in cortex. Scale bar = 100 μm for **A**, and 200 μm for **B**. **C**, Quantification of cortex neuropil 6E10 plaque staining expressed as the average percentage of area occupied by 6E10-positive manually traced diffuse plaques per total area analyzed \pm SEM ($n \geq 50$ for 6E10, 2-3 animals per transgenic group). NS indicates no statistically significant difference detected compared to APPSwDI/NOS2^{-/-} untreated control group ($p > 0.1$ from one-way ANOVA test). *** = $p < 0.0001$ (one-way ANOVA + Tukey's post-hoc analysis).

neuropathology expected in APPSwDI/NOS2^{-/-} transgenic mice model. Both degenerating soma and filamentous dystrophic neurites were observed to emerge from pyramidal cell layer, and they were often engulfed in phagocytic glia. Similarly, lipofuscin bodies, the hallmark sign of aging brains were encountered in cytoplasm of APP brains (Supplementary Fig. S2 and Fig. 6G), as well as in degenerating or phagocytosed elements (Fig. 6B and 6D), and associated with multilamellar bodies (Fig. 6E). Myelin capsulated dystrophic neurites, containing bundled fibrils, phagocytic vacuoles, or electron dense contents with limiting membranes, and somatoplasmic pathologies were also encountered in neuropil regions of striatum radiatum, both in APP Control and APP BBG brains (Supplementary Fig. S2), suggesting that BBG treatment did not affect the filamentous pathology in hippocampal dendrites. Without using phospho-tau immunostaining, we cannot ascertain whether or not filament pathology we observe using electron microscopy in 9 months of age brains is related to tau pathology that was previously demonstrated in this transgenic model at one years of age using light microscopy [3]. It should be worthwhile to investigate effects of BBG treatment on tau pathology as a follow-up study, in order to further evaluate therapeutic feasibility of BBG treatment in human AD, where tau-phosphorylation is the strongest predictor of cell death. The most drastic qualitative difference between the APP Control and APP BBG brains was considerably reduced instances of

degenerating cell remnants among the pyramidal somata (Fig. 6A vs. 6B), although more subtle differences in prevalence of neuropathologies listed above, or the differences in intracellular or extracellular peptide localization, cannot be revealed without quantitative immuno EM analysis, which is not employed in the current study. Nevertheless, the EM observations also confirmed our light microscopy analysis indicating that the BBG treatment particularly intervenes before substantial cell death takes place in the hippocampus of APPSwDI/NOS2^{-/-} brains.

DISCUSSION

In this study, we quantified the effect of 2,000 mg/kg/day BBG oral administration of the triphenylmethane dye BBG on cell survival and APP/A β accumulation in APPSwDI/NOS2^{-/-} mice, a transgenic model of AD. We demonstrated that oral BBG had significant effects on neuron survival and intracellular APP/A β accumulation in the hippocampus. In contrast, amyloid plaques in the cortex neuropil were not affected by BBG treatment. While ultrastructural examination of hippocampal circuitry revealed pathological elements that were hallmark signs of AD in both untreated and treated brains, oral BBG treatment reduced the instances of hippocampal cells that contained varying stages of degeneration products. These results suggest that BBG is potentially an effective agent to prevent progression of a key hallmark sign of AD, neuronal loss.

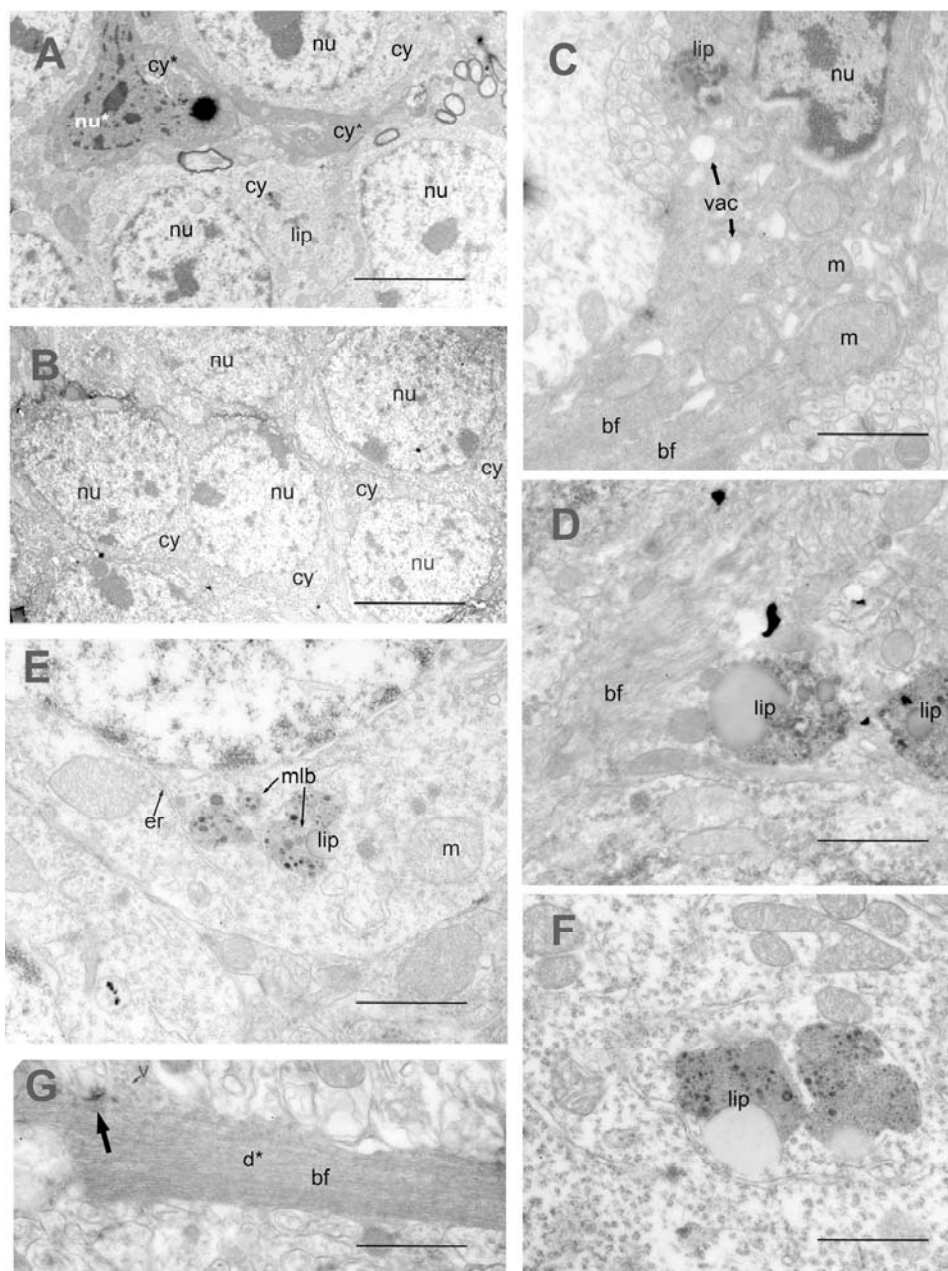


Fig. (6). Ultrastructural displays of neuronal pathology in APPSwDI/NOS2^{-/-} mice that were untreated (A, C, D, F, G) or treated (B, E) with BBG. **A**, Degenerating cells displaying dark chromatin, ovoid or irregularly shaped nucleus (nu*) and electron dense cytoplasm (cy*), indicating degeneration, mottle CA1 pyramidal cell layers in untreated brains. **B**, In BBG treated brains, occurrence of such degenerating cells was rare. **C**, Higher magnification views of degenerating cytoplasm in untreated brains reveal vacuoles (vac), swollen or vacuuous mitochondria (mit), and lipofuscin (lip) deposits. Bundled filaments (bf) were also common. **D-F**, Bundled filaments (bf) and lipofuscin (lip) deposits, with or without osmiophobic (i.e., low contrast in EM images), possibly proteinaceous components were also encountered in cytoplasm of non-degenerating cells of both BBG treated (E) and untreated (D, F) brains. Small osmiophilic granules and osmiophobic components of lipofuscin are often aggregated as multilamellar bodies (mlb; E). **G**, Bundled filaments (bf) in degenerating neurons of BBG untreated brains filled degenerating dendritic processes (d*); it was possible to find synapses (arrow) on these dendrites suggesting that filament pathology precedes deafferentation of neurons destined to degenerate. Scale bars displayed = 10 μ m in **A** and **B**, 2 μ m in **C** and **E**, and 1 μ m in **D**, **F**, and **G**.

Bioavailability of BBG in Wild Type and AD Mice

The quantification of BBG concentration in the brain-tissue revealed that the dye could cross the blood-brain barrier (BBB) in APPSwDI/NOS2^{-/-} familial AD-transgenic mice, but not in wild type control mice. Passage of therapeu-

tic molecules across the BBB in Alzheimer's Disease (AD) is a highly complex phenomena, with differing degrees of BBB disruption being reported in the literature from studies with AD mouse models [74]. For example, previous studies with multiple transgenic mouse models of AD have shown a

lack of widespread BBB disruption measured by negligible BBB permeability of larger molecular weight species, including therapeutic antibodies, and also some smaller molecular weight compounds [74]. Nevertheless, our current finding is consistent with previous observations of increased BBB permeability in certain specific transgenic mouse models [18, 44] and that in AD, increased CNS infiltration of inflammatory cells/immunoglobulins [44, 46, 75] and peripheral blood proteins [16,75,76] has been observed. Deletion of nitric oxide synthase in the APPSwDI/NOS2-/- mouse model decreases protection against immune response, allowing for increased inflammation [22] and potential leakage of the BBB in the AD brain [44]. The APPSwDI/NOS2-/- mouse also exhibits decreased aquaporin 4 and glial fibrillary acid protein astrocytic end feet, both of which are features required for the integrity of the BBB [26, 77, 78]. In addition, the neurovascular blood-brain barrier has been demonstrated to undergo disruption and dysfunction in other neurodegenerative diseases [44, 75, 76]. For example, in rodent models of traumatic brain injury [28] and spinal cord injury [34, 39], peripherally administered BBG was found to accumulate at the contusion site, indicating that the compound was able to access the brain through the disrupted BBB. Although BBB permeability of BBG in human brain at different stages of AD progression remains a pharmacokinetic challenge, the BBB permeability of orally administered 2,000 mg/kg/day BBG in a transgenic AD model strengthens the potential pharmaceutical potency of this compound as a therapeutic agent. Since the 2,000 mg/kg/day dosage utilized in our study was well-tolerated and the maximum safe dosage of orally administered BBG into mice reported so far was 3,500 mg/kg/day BBG [28], it is expected that a higher dosage of oral BBG could be utilized in future studies.

Significance of BBG's Effect on Neuronal Loss in AD

We demonstrated that BBG effectively reduced AD-related neuronal loss in the hippocampus of a transgenic model. Because not all AD-mouse models develop significant neuronal loss [79], this pathological endpoint is often excluded from efficacy studies of new therapeutics. However, neuronal loss in hippocampus, a brain region critical for learning, memory consolidation, and spatial navigation [80, 81] is chiefly responsible for loss of cognitive function in AD. Because therapeutics that prevent AD-related neuronal loss also enhance cognitive/behavioral function [19, 20, 82-85], the demonstration of BBG's effectiveness to alleviate cell loss in the subiculum and CA1-CA2 regions in the current study emphasizes the potency of this compound as a promising agent in the treatment of AD.

The Effect of BBG on APP/A β Accumulation

We have demonstrated that oral BBG administration significantly reduced 6E10 APP/A β staining prominently in or around somata in hippocampal pyramidal cells. Aggregated species of secreted A β found in the extracellular space were hypothesized to initiate the cascade of events in the toxicity that leads to amyloid plaques [63]. There is also evidence that the neurodegenerative cascade may be triggered by A β accumulation inside neurons [86]. Indeed, recent studies have demonstrated that neuronal loss, cognitive decline, and

synapse degradation can occur independent from the appearance of plaques in the AD brain neuropil, and that intracellular A β coincides better with these pathological events [54, 55, 60, 64, 66, 67, 87-91]. In fact, it was reported that the formation of A β oligomers and fibrils actually begins by internalized A β monomer being sorted to multivesicular bodies inside of cells, where aggregation then proceeds. The aggregates are then only released to the extracellular space once the cells undergo cell death [52, 92, 93]. Furthermore, intracellular A β has been found to be many times more toxic than extracellular A β in the neuropil [94]. Although further study is required to confirm the exact identity of the stained APP/A β species (parent APP protein, A β , alternate cleavage product, or aggregated) and confirm whether BBG is truly affecting the A β pathological hallmark of AD, the concurrent reduction of intracellular 6E10 staining and neuronal death with BBG administration is in agreement with the hypothesis that post-cleavage APP fragments in the intracellular space is a crucial step in cascade of events leading to neurodegeneration in AD brains.

It should also be noted that anti-inflammatory actions of BBG may share responsibility in alleviation of AD pathology in transgenic models. In J20 hAPP transgenic mice, BBG reduces A β plaques by promoting non-amyloidogenic processing of A β PP by alpha-secretase through the P2X7 receptor [18], while BBG also prevents *in vitro* A β aggregation with an alpha-secretase independent mechanism [8].

Our findings that the effect of BBG on APP/A β accumulation is more detectable at the hippocampal cell layer, and the oral BBG treatment impacts not the occurrences of intracellular multivesicular bodies and dystrophic neurites, but the cellular degeneration due to excessive APP/A β and filament accumulation, indicate that BBG likely interferes with A β pathogenesis at the stage when A β is intracellular. Furthermore, our results also indicate that the effect of BBG on hippocampal cell death is not simply via delaying the death of cells that have accumulated considerable APP/A β , but via preventing the APP/A β accumulation in the cells prior to trigger of cell death cascade. If BBG's effect to reduce APP/A β in APPSwDI/NOS2-/- brains was due primarily to its P2X7 receptor antagonism mediated anti-inflammatory action in preventing microglial activation and phagocytic activity [39,95], then the prevention of neuronal numbers with BBG would have led to increased APP/A β in these brains. We have found the exact opposite; BBG treatment prevents neuronal loss while reducing the APP/A β amounts in the pyramidal cell layer. This is most likely explained through a mechanism by which BBG prevents the formation or entry of A β into hippocampal cells, thereby preventing A β 's efficacy to kill the neurons.

Then, through what mechanism BBG was able to reduce intracellular APP/A β 6E10 staining in our study? Was it through inhibition of A β aggregation, inhibition of A β monomer generation from the APP parent protein, or preventing entry of A β in to neurons? All of these mechanisms are possible based on the findings in the current study, as additional valuable investigations aimed at identifying the stained intracellular APP/A β 6E10 species (as parent APP protein, A β , alternate cleavage product, or aggregated

isoform) are required to confirm the specific mechanism. If BBG acts by a mechanism that inhibits intracellular A β aggregation, BBG treatment would be expected to reduce A β staining in neurons. The finding that 6E10 staining in hippocampal neurons is reduced upon BBG treatment is consistent with this expectation. Our previous findings using *in vitro* models also supports this mechanism [8]. Then, the question is whether this inhibition occurs intracellularly or extracellularly. BBG has a relatively large molecular weight (854 Da) and is hydrophilic, two properties that potentially hinder the permeability of this compound through the cell membrane. Therefore, we speculate that an intracellular site of action for BBG inhibiting A β aggregation is unlikely. Extracellularly, BBG may inhibit A β monomer generation from the APP parent protein [18, 96], it may simply block the entry of A β in to neurons [97], or by simply inhibiting formation A β oligomers in the extracellular domain, it disrupts a mechanism in which A β oligomers need to re-enter the cell to start a cascade of events that lead to cell death. This latter possibility is further compelling in that it also fits with our current finding that BBG reduced the amount to pan-amyloid 6E10 staining in neurons that were spared from cell death.

The current study demonstrated that BBG treatment led to a reduction in intracellular 6E10 staining, but not in the size or extent of the APP/A β plaques. A possible explanation for this discrepancy is that BBG may be more efficacious at inhibiting the formation of new aggregates, leaving existing large-volume aggregates and post-degeneration products unaffected. The second possibility is that the transgenic mice used in our study were at a young age, prior to having accumulated enough A β neuropil plaque pathology to detect differences upon application of the BBG compound. For example, the initial validation of the APPSwDI/NOS2 $^{-/-}$ strain using 12-14 month mice revealed extensive A β deposits in the neuropil, but a lack of intracellular A β stain [3]. Since the mice used in our study were 9-10 months at the time of analysis and it has been reported that intracellular A β appears first in the aging process followed by decline and an inversely proportional increase in the number and the size of A β plaques [53], it is quite possible that extent of A β plaque pathology and the effect of BBG treatment on this pathology were below the threshold for detection with the techniques used in the current study.

CONCLUSION

To our knowledge, our investigation on the oral administration of BBG in APPSwDI/NOS2 $^{-/-}$ familial AD mice is the first report of 1) the effect of this compound on neuronal loss in a transgenic animal model of AD, 2) a protein conformation/aggregation disease is affected via oral administration of BBG, and 3) electron microscopic ultrastructural analysis of AD pathology in APPSwDI/NOS2 $^{-/-}$ mice. Because BBG improved a key biochemical AD pathology (loss of neurons), the next step should be to proceed with behavioral studies with AD transgenic mice to determine if it can also improve AD-associated cognitive decline/function. Furthermore, the finding that the reduction of intracellular APP/A β and the neuronal loss were achieved via an extracellular site of

action highlights extracellular A β monomers as a promising potential target for AD therapeutics development. Lastly, the current results enhance our understanding of the food dye analog-based small molecules as effective APP/A β modulators in physiologically relevant *in vivo* systems.

AUTHOR CONTRIBUTIONS

J.A.I performed animal handling, Brilliant Blue G administration, tissue processing, and immunohistochemical staining, imaging, and quantification. J.A.I and I.K. performed biochemical quantification of Brilliant Blue G in brain tissue. A.E contributed in experimental design and in planning for neuroanatomical data collection and analysis, and performed electron microscopy tissue preparation and analysis. J.A.I, A.E, and I.K. discussed and analyzed results and wrote manuscript.

FUNDING SOURCES

This study was supported by National Science Foundation Graduate Research Fellowship (DGE-00809128) to J.I., and in part by Award No. 13-6 from the Commonwealth of Virginia's Alzheimer's and Related Diseases Research Award Fund, administered by the Virginia Center on Aging, Virginia Commonwealth University to I.K. The authors acknowledge financial support from the National Research Foundation of Korea (NRF) funded by the Ministry of Science, ICT & Future Planning (Grant No. 2014R1A2A1A11050322). This work was supported by the BioImaging Research Center at the Gwangju Institute of Science and Technology (GIST), Korea. The funders had no role in study design, data collection and analysis, decision to publish, or preparation of the manuscript.

SUPPLEMENTARY MATERIAL

Supplementary Fig. S1 (neuronal quantification approach employed) and S2 (Ultrastructural pathology in APPSwDI/NOS2 $^{-/-}$ mice brains) are available for access and download online at the Current Alzheimer's Research website.

Supplementary material is available on the publisher's web site along with the published article.

CONFLICT OF INTEREST

The authors confirm that this article content has no conflict of interest.

ACKNOWLEDGEMENTS

We wish to acknowledge, Professor George Bloom, Eric Swanson, and Genrieta Bochorishvili of University of Virginia's Department of Biology and Psychology, respectively, for valuable discussion and insight regarding APPSwDI/NOS2 $^{-/-}$ transgenic mice and development of light-level immunohistochemical assays. Lastly, we wish to acknowledge the lab of Professor Carol Colton from Duke University Medical Center's Division of Neurology for original development of the APPSwDI/NOS2 $^{-/-}$ mouse model.

REFERENCES

- [1] LaFerla FM, Green KN. Animal models of Alzheimer disease. *Cold Spring Harb Perspect Med* 2(11): a006320-0 (2012).
- [2] Nagy ZS, Esiri MM, Joachim C, Jobst KA, Morris JH, King EM, *et al.* Comparison of pathological diagnostic criteria for Alzheimer disease. *Alzheimer Dis Assoc Disord* 12(3): 182-9 (1998).
- [3] Wilcock DM, Lewis MR, Van Nostrand WE, Davis J, Previti ML, Gharkholonarehe N, *et al.* Progression of amyloid pathology to Alzheimer's disease pathology in an amyloid precursor protein transgenic mouse model by removal of nitric oxide synthase 2. *J Neurosci* 28(7): 1537-45 (2008).
- [4] Hardy J, Selkoe DJ. The amyloid hypothesis of Alzheimer's disease: progress and problems on the road to therapeutics. *Science* 297(5580): 353-6 (2002).
- [5] Hamaguchi T, Ono K, Yamada M. Anti-amyloidogenic therapies: strategies for prevention and treatment of Alzheimer's disease. *Cell Mol Life Sci* 63(13): 1538-52 (2006).
- [6] Necula M, Kaye R, Milton S, Glabe CG. Small molecule inhibitors of aggregation indicate that amyloid beta oligomerization and fibrillization pathways are independent and distinct. *J Biol Chem* 282(14): 10311-24 (2007).
- [7] Irwin JA, Wong HE, Kwon I. Different fates of Alzheimer's disease amyloid- β fibrils remodeled by biocompatible small molecules. *Biomacromolecules* 14(1): 264-74 (2013).
- [8] Wong HE, Qi W, Choi H-M, Fernandez EJ, Kwon I. A safe, blood-brain barrier permeable triphenylmethane dye inhibits amyloid- β neurotoxicity by generating nontoxic aggregates. *ACS Chem Neurosci* 2(11): 645-57 (2011).
- [9] Takenouchi T, Sekiyama K, Sekigawa A, Fujita M, Waragai M, Sugama S, *et al.* P2X7 receptor signaling pathway as a therapeutic target for neurodegenerative diseases. *Arch Immunol Ther Exp (Warsz)* 58(2): 91-6 (2010).
- [10] Cervetto C, Frattaroli D, Maura G, Marcoli M. Motor neuron dysfunction in a mouse model of ALS: gender-dependent effect of P2X7 antagonism. *Toxicology* 311(1-2): 69-77 (2013).
- [11] Sperlágh B, Illes P. P2X7 receptor: an emerging target in central nervous system diseases. *Trends Pharmacol Sci* 35(10): 537-47 (2014).
- [12] Carmo MRS, Menezes APF, Nunes ACL, Pliássova A, Rolo AP, Palmeira CM, *et al.* The P2X7 receptor antagonist Brilliant Blue G attenuates contralateral rotations in a rat model of Parkinsonism through a combined control of synaptotoxicity, neurotoxicity and gliosis. *Neuropharmacology* 81:142-52 (2014).
- [13] Iwamaru Y, Takenouchi T, Murayama Y, Okada H, Imamura M, Shimizu Y, *et al.* Anti-prion activity of Brilliant Blue G. *PLoS One* 7(5): e37896 (2012).
- [14] Díaz-Hernández M, Díez-Zaera M, Sánchez-Nogueiro J, Gómez-Villafuertes R, Canals JM, Alberch J, *et al.* Altered P2X7-receptor level and function in mouse models of Huntington's disease and therapeutic efficacy of antagonist administration. *FASEB J* 23(6): 1893-906 (2009).
- [15] Miras-Portugal MT, Diaz-Hernandez JI, Gomez-Villafuertes R, Diaz-Hernandez M, Artalejo AR, Gualix J. Role of P2X7 and P2Y2 receptors on α -secretase-dependent APP processing: Control of amyloid plaques formation "in vivo" by P2X7 receptor. *Comp Struc Biotechnol J* 13: 176-81 (2015).
- [16] Ryu JK, McLarnon JG. Block of purinergic P2X(7) receptor is neuroprotective in an animal model of Alzheimer's disease. *Neuroreport* 19(17): 1715-9 (2008).
- [17] Chen X, Hu J, Jiang L, Xu S, Zheng B, Wang C, *et al.* Brilliant Blue G improves cognition in an animal model of Alzheimer's disease and inhibits amyloid- β -induced loss of filopodia and dendrite spines in hippocampal neurons. *Neuroscience* 279: 94-101 (2014).
- [18] Diaz-Hernandez JI, Gomez-Villafuertes R, León-Otegui M, Hontecillas-Prieto L, Del Puerto A, Trejo JL, *et al.* In vivo P2X7 inhibition reduces amyloid plaques in Alzheimer's disease through GSK3 β and secretases. *Neurobiol Aging* 33(8): 1816-28 (2012).
- [19] Sudduth TL, Wilson JG, Everhart A, Colton CA, Wilcock DM. Lithium treatment of APPSwDI/NOS2 $^{-/-}$ mice leads to reduced hyperphosphorylated tau, increased amyloid deposition and altered inflammatory phenotype. *PLoS One* 7(2): e31993 (2012).
- [20] Wilcock DM, Gharkholonarehe N, Van Nostrand WE, Davis J, Vitek MP, Colton CA. Amyloid reduction by amyloid-beta vaccination also reduces mouse tau pathology and protects from neuron loss in two mouse models of Alzheimer's disease. *J Neurosci* 29(25): 7957-65 (2009).
- [21] Nussbaum JM, Schilling S, Cynis H, Silva A, Swanson E, Wangsanut T, *et al.* Prion-like behaviour and tau-dependent cytotoxicity of pyroglutamylated amyloid- β . *Nature* 485(7400): 651-5 (2012).
- [22] Mestas J, Hughes C. Of mice and not men: differences between mouse and human immunology. *J Immunol* 172(5): 2731-8 (2004).
- [23] Kummer MP, Hermes M, Delekarte A, Hammerschmidt T, Kumar S, Terwel D, *et al.* Nitration of tyrosine 10 critically enhances amyloid β aggregation and plaque formation. *Neuron* 71(5): 833-44 (2011).
- [24] Nathan C, Calingasan N, Nezezon J, Ding A, Lucia MS, La Perle K, *et al.* Protection from Alzheimer's-like disease in the mouse by genetic ablation of inducible nitric oxide synthase. *J Exp Med* 202(9): 1163-9 (2005).
- [25] Ridnour LA, Dhanapal S, Hoos M, Wilson J, Lee J, Cheng RYS, *et al.* Nitric oxide-mediated regulation of β -amyloid clearance via alterations of MMP-9/TIMP-1. *J Neurochem* 123(5): 736-49 (2012).
- [26] Wilcock DM, Vitek MP, Colton CA. Vascular amyloid alters astrocytic water and potassium channels in mouse models and humans with Alzheimer's disease. *Neuroscience* 159(3): 1055-69 (2009).
- [27] Young CNJ, Brutkowski W, Lien C-F, Arkle S, Lochmüller H, Zablocki K, *et al.* P2X7 purinoceptor alterations in dystrophic mdx mouse muscles: relationship to pathology and potential target for treatment. *J Cell Mol Med* 16(5): 1026-37 (2012).
- [28] Kimbler DE, Shields J, Yanasak N, Vender JR, Dhandapani KM. Activation of P2X7 promotes cerebral edema and neurological injury after traumatic brain injury in mice. *PLoS One* 7(7): e41229 (2012).
- [29] Borzelleca JF, Depukat K, Hallagan JB. Lifetime toxicity/carcinogenicity studies of FD & C blue No. 1 (Brilliant blue FCF) in rats and mice. *Food Chem Toxicol Pergamon* 28(4): 221-34 (1990).
- [30] Kukar T, Prescott S, Eriksen JL, Holloway V, Murphy MP, Koo EH, *et al.* Chronic administration of R-flurbiprofen attenuates learning impairments in transgenic amyloid precursor protein mice. *BMC Neurosci* 8: 54 (2007).
- [31] Hawkes CA, Deng L-H, Shaw JE, Nitz M, McLaurin J. Small molecule beta-amyloid inhibitors that stabilize protofibrillar structures *in vitro* improve cognition and pathology in a mouse model of Alzheimer's disease. *Eur J Neurosci* 31(2): 203-13 (2010).
- [32] Medina DX, Caccamo A, Oddo S. Methylene blue reduces a β levels and rescues early cognitive deficit by increasing proteasome activity. *Brain Pathol* 21(2): 140-9 (2011).
- [33] Zhang J, Zhen Y-F, Pu-Bu-Ci-Ren, Song L-G, Kong W-N, Shao T-M, *et al.* Salidroside attenuates beta amyloid-induced cognitive deficits via modulating oxidative stress and inflammatory mediators in rat hippocampus. *Behav Brain Res* 244:70-81 (2013).
- [34] Parthasarathy V, McClean PL, Hölscher C, Taylor M, Tinker C, Jones G, *et al.* A novel retro-inverso peptide inhibitor reduces amyloid deposition, oxidation and inflammation and stimulates neurogenesis in the APPsw/PS1 Δ E9 mouse model of Alzheimer's disease. *PLoS One* 8(1): e54769 (2013).
- [35] Murata N, Murakami K, Ozawa Y, Kinoshita N, Irie K, Shirasawa T, *et al.* Silymarin attenuated the amyloid β plaque burden and improved behavioral abnormalities in an Alzheimer's disease mouse model. *Biosci Biotechnol Biochem* 74(11): 2299-306 (2010).
- [36] Chan J, Aoki C. Optimization of differential immunogold-silver and peroxidase labeling with maintenance of ultrastructure in brain sections before plastic embedding. *J Neurosci Methods* 33(2-3): 113-27 (1990).
- [37] Corson JA, Nahmani M, Lubarsky K, Badr N, Wright C, Erisir A. Sensory activity differentially modulates N-methyl-D-aspartate receptor subunits 2A and 2B in cortical layers. *Neuroscience* 163(3): 920-32 (2009).
- [38] Erisir A, Dreusicke M. Quantitative morphology and postsynaptic targets of thalamocortical axons in critical period and adult ferret visual cortex. *J Comp Neurol* 485(1): 11-31 (2005).
- [39] Peng W, Cotrina ML, Han X, Yu H, Bekar L, Blum L, *et al.* Systemic administration of an antagonist of the ATP-sensitive receptor P2X7 improves recovery after spinal cord injury. *Proc Natl Acad Sci USA* 106(30): 12489-93 (2009).
- [40] Bieschke J, Herbst M, Wiglenda T, Friedrich RP, Boeddrich A, Schiele F, *et al.* Small-molecule conversion of toxic oligomers to nontoxic β -sheet-rich amyloid fibrils. *Nat Chem Biol* 8(1): 93-101 (2012).

- [41] Calon F, Lim GP, Yang F, Morihara T, Teter B, Ubeda O, *et al.* Docosahexaenoic acid protects from dendritic pathology in an Alzheimer's disease mouse model. *Neuron* 43(5): 633-45 (2004).
- [42] Moreno-Gonzalez I, Estrada LD, Sanchez-Mejias E, Soto C. Smoking exacerbates amyloid pathology in a mouse model of Alzheimer's disease. *Nat Comm* 4: 1495 (2013).
- [43] Ghosal K, Vogt DL, Liang M, Shen Y, Lamb BT, Pimplikar SW. Alzheimer's disease-like pathological features in transgenic mice expressing the APP intracellular domain. *Proc Natl Acad Sci USA* 106(43): 18367-72 (2009).
- [44] Ryu JK, McLarnon JG. A leaky blood-brain barrier, fibrinogen infiltration and microglial reactivity in inflamed Alzheimer's disease brain. *J Cell Mol Med* 13(9A): 2911-25 (2009).
- [45] Dinamarca MC, Arrázola M, Toledo E, Cerpa WF, Hancke J, Inestrosa NC. Release of acetylcholinesterase (AChE) from beta-amyloid plaques assemblies improves the spatial memory impairments in APP-transgenic mice. *Chem Biol Interact* 175(1-3): 142-9 (2008).
- [46] Cheng Z, Zhang J, Liu H, Li Y, Zhao Y, Yang E. Central nervous system penetration for small molecule therapeutic agents does not increase in multiple sclerosis- and Alzheimer's disease-related animal models despite reported blood-brain barrier disruption. *Drug Metab Dispos* 38(8):1355-61 (2010).
- [47] Pardridge WM. Drug transport across the blood-brain barrier. *J Cereb Blood Flow Metab* 32(11): 1959-72 (2012).
- [48] Green FJ. The Sigma-Aldrich Handbook of Stains, Dyes, and Indicators. Milwaukee, WI: Aldrich Chem Company Library, p. 1 (1990).
- [49] Bell RD, Ehlers MD. Breaching the blood-brain barrier for drug delivery. *Neuron* 81(1):1-3 (2014).
- [50] Wright AL, Zinn R, Hohensinn B, Konen LM, Beynon SB, Tan RP, *et al.* Neuroinflammation and neuronal loss precede A β plaque deposition in the hAPP-J20 mouse model of Alzheimer's disease. *PLoS One* 8(4): e59586 (2013).
- [51] Green KN, Billings LM, Roozendaal B, McLaugh JL, LaFerla FM. Glucocorticoids increase amyloid-beta and tau pathology in a mouse model of Alzheimer's disease. *J Neurosci* 26(35): 9047-56 (2006).
- [52] Oddo S, Caccamo A, Tran L, Lambert MP, Glabe CG, Klein WL, *et al.* Temporal profile of amyloid-beta (A β) oligomerization in an *in vivo* model of Alzheimer disease. A link between A β and tau pathology. *J Biol Chem* 281(3): 1599-604 (2006).
- [53] Oddo S, Caccamo A, Smith IF, Green KN, LaFerla FM. A dynamic relationship between intracellular and extracellular pools of A β . *Am J Pathol* 168(1):184-94 (2006).
- [54] Mastrangelo MA, Bowers WJ. Detailed immunohistochemical characterization of temporal and spatial progression of Alzheimer's disease-related pathologies in male triple-transgenic mice. *BMC Neurosci* 9: 81 (2008).
- [55] Billings LM, Oddo S, Green KN, McLaugh JL, LaFerla FM. Intra-neuronal A β causes the onset of early Alzheimer's disease-related cognitive deficits in transgenic mice. *Neuron* 45(5): 675-88 (2005).
- [56] Hirata-Fukae C, Li H-F, Hoe H-S, Gray AJ, Minami SS, Hamada K, *et al.* Females exhibit more extensive amyloid, but not tau, pathology in an Alzheimer transgenic model. *Brain Res* 1216: 92-103 (2008).
- [57] Gouras GK, Willén K, Tampellini D. Critical role of intraneuronal A β in Alzheimer's disease: technical challenges in studying intracellular A β . *Life Sci* 91(23-24): 1153-8 (2012).
- [58] Wirths O, Bayer TA. Intra-neuronal A β accumulation and neurodegeneration: lessons from transgenic models. *Life Sci* 1(23-24): 1148-52 (2012).
- [59] Gouras GK, Almeida CG, Takahashi RH. Intra-neuronal A β accumulation and origin of plaques in Alzheimer's disease. *Neurobiol Aging* 26(9): 1235-44 (2005).
- [60] Philipson O, Lannfelt L, Nilsson LNG. Genetic and pharmacological evidence of intraneuronal A β accumulation in APP transgenic mice. *FEBS Lett* 583(18): 3021-6 (2009).
- [61] Lord A, Kalimo H, Eckman C, Zhang X-Q, Lannfelt L, Nilsson LNG. The Arctic Alzheimer mutation facilitates early intraneuronal A β aggregation and senile plaque formation in transgenic mice. *Neurobiol Aging* 27(1): 67-77 (2006).
- [62] Aho L, Pikkarainen M, Hiltunen V, Leinonen V, Alafuzoff I. Immunohistochemical visualization of amyloid-beta protein precursor and amyloid-beta in extra- and intracellular compartments in the human brain. *J Alzheimers Dis* 20(4): 1015-28 (2010).
- [63] Bayer TA, Wirths O. Intracellular accumulation of amyloid-Beta - a predictor for synaptic dysfunction and neuron loss in Alzheimer's disease. *Front Aging Neurosci* 2: 8 (2010).
- [64] Umeda T, Tomiyama T, Sakama N, Tanaka S, Lambert MP, Klein WL, *et al.* Intra-neuronal amyloid β oligomers cause cell death via endoplasmic reticulum stress, endosomal/lysosomal leakage, and mitochondrial dysfunction *in vivo*. *J Neurosci Res* 89(7): 1031-42 (2011).
- [65] Tomiyama T, Matsuyama S, Iso H, Umeda T, Takuma H, Ohnishi K, *et al.* A mouse model of amyloid beta oligomers: their contribution to synaptic alteration, abnormal tau phosphorylation, glial activation, and neuronal loss *in vivo*. *J Neurosci* 30(14): 4845-56 (2010).
- [66] Oakley H, Cole SL, Logan S, Maus E, Shao P, Craft J, *et al.* Intra-neuronal beta-amyloid aggregates, neurodegeneration, and neuron loss in transgenic mice with five familial Alzheimer's disease mutations: potential factors in amyloid plaque formation. *J Neurosci* 26(40): 10129-40 (2006).
- [67] Crowther DC, Kinghorn KJ, Miranda E, Page R, Curry JA, Duthie FAI, *et al.* Intra-neuronal A β , non-amyloid aggregates and neurodegeneration in a Drosophila model of Alzheimer's disease. *Neuroscience* 132(1):123-35 (2005).
- [68] Martiniere W, Kuperstein I, Wilkinson H, Maes E, Vanbrabant M, Jonckheere W, *et al.* Lipids revert inert A β amyloid fibrils to neurotoxic protofibrils that affect learning in mice. *EMBO J* 27(1): 224-33 (2008).
- [69] LaFerla FM, Green KN, Oddo S. Intracellular amyloid-beta in Alzheimer's disease. *Nat Rev Neurosci* 8(7): 499-509 (2007).
- [70] Wirths O, Multhaup G, Bayer TA. A modified beta-amyloid hypothesis: intra-neuronal accumulation of the beta-amyloid peptide--the first step of a fatal cascade. *J Neurochem* 91(3): 513-20 (2004).
- [71] Goodman TF, Abele DC, West CS. Electron microscopy in the diagnosis of amyloidosis. *Arch Dermatol* 106(3): 393-7 (1972).
- [72] Perl DP. Neuropathology of Alzheimer's Disease. *Mt Sinai J Med* 77(1): 32-42 (2010).
- [73] Sanchez-Varo R, Trujillo-Estrada L, Sanchez-Mejias E, Torres M, Baglietto-Vargas D, Moreno-Gonzalez I, *et al.* Abnormal accumulation of autophagic vesicles correlates with axonal and synaptic pathology in young Alzheimer's mice hippocampus. *Acta Neuropathol* 123(1): 53-70 (2012).
- [74] Bien-Ly N, Boswell CA, Jeet S, Beach TG, Hoyte K, Luk W, *et al.* Lack of widespread BBB disruption in Alzheimer's disease models: focus on therapeutic antibodies. *Neuron* 88(2): 289-97 (2015).
- [75] Erickson MA, Banks WA. Blood-brain barrier dysfunction as a cause and consequence of Alzheimer's disease. *J Cereb Blood Flow Metab* 33(10): 1500-13 (2013).
- [76] Banks WA. Drug delivery to the brain in Alzheimer's disease: consideration of the blood-brain barrier. *Adv Drug Deliv Rev* 64(7): 629-39 (2012).
- [77] Liu L, Su Y, Yang W, Xiao M, Gao J, Hu G. Disruption of neuronal-glia-vascular units in the hippocampus of ovariectomized mice injected with D-galactose. *Neuroscience* 169(2): 596-608 (2010).
- [78] Zhou J, Kong H, Hua X, Xiao M, Ding J, Hu G. Altered blood-brain barrier integrity in adult aquaporin-4 knockout mice. *Neuroreport* 19(1):1-5 (2008).
- [79] Eriksen JL, Janus CG. Plaques, tangles, and memory loss in mouse models of neurodegeneration. *Behav Genet* 7(1):79-100 (2007).
- [80] Mu Y, Gage FH. Adult hippocampal neurogenesis and its role in Alzheimer's disease. *Mol Neurodegener* 6: 85 (2011).
- [81] Intlekofer KA, Cotman CW. Exercise counteracts declining hippocampal function in aging and Alzheimer's disease. *Neurobiol Dis* 57: 47-55 (2013).
- [82] Serenó L, Coma M, Rodríguez M, Sánchez-Ferrer P, Sánchez MB, Gich I, *et al.* A novel GSK-3 β inhibitor reduces Alzheimer's pathology and rescues neuronal loss *in vivo*. *Neurobiol Dis* 35(3): 359-67 (2009).
- [83] Nunes AF, Amaral JD, Lo AC, Fonseca MB, Viana RJS, Callaerts-Vegh Z, *et al.* TUDCA, a bile acid, attenuates amyloid precursor protein processing and amyloid- β deposition in APP/PS1 mice. *Mol Neurobiol* 5(3): 440-54 (2012).
- [84] Butovsky O, Koronyo-Hamaoui M, Kunis G, Ophir E, Landa G, Cohen H, *et al.* Glatiramer acetate fights against Alzheimer's dis-

- ease by inducing dendritic-like microglia expressing insulin-like growth factor 1. *Proc Natl Acad Sci USA* 103(31): 11784-9 (2006).
- [85] Dong H, Goico B, Martin M, Csernansky CA, Bertchume A, Csernansky JG. Modulation of hippocampal cell proliferation, memory, and amyloid plaque deposition in APPsw (Tg2576) mutant mice by isolation stress. *Neuroscience* 127(3): 601-9 (2004).
- [86] Gouras GK, Tampellini D, Takahashi RH, Capetillo-Zarate E. Intra-neuronal beta-amyloid accumulation and synapse pathology in Alzheimer's disease. *Acta Neuropathol* 119(5): 523-41 (2010).
- [87] Tampellini D, Rahman N, Gallo EF, Huang Z, Dumont M, Capetillo-Zarate E, *et al.* Synaptic activity reduces intra-neuronal Abeta, promotes APP transport to synapses, and protects against Abeta-related synaptic alterations. *J Neurosci* 29(31): 9704-13 (2009).
- [88] Knobloch M, Konietzko U, Krebs DC, Nitsch RM. Intracellular Abeta and cognitive deficits precede beta-amyloid deposition in transgenic arcAbeta mice. *Neurobiol Aging* 28(9): 1297-306 (2007).
- [89] Casas C, Sergeant N, Itier J-M, Blanchard V, Wirths O, van der Kolk N, *et al.* Massive CA1/2 neuronal loss with intra-neuronal and N-terminal truncated Abeta42 accumulation in a novel Alzheimer transgenic model. *Am J Pathol* 165(4): 1289-300 (2004).
- [90] Kienlen-Campard P, Miolet S, Tasiaux B, Octave J-N. Intracellular amyloid-beta 1-42, but not extracellular soluble amyloid-beta peptides, induces neuronal apoptosis. *J Biol Chem* 277(18):15666-70 (2002).
- [91] Gouras GK, Tsai J, Naslund J, Vincent B, Edgar M, Checler F, *et al.* Intra-neuronal Abeta42 accumulation in human brain. *Am J Pathol* 156(1): 15-20 (2000).
- [92] Friedrich RP, Tepper K, Rönicke R, Soom M, Westermann M, Reymann K, *et al.* Mechanism of amyloid plaque formation suggests an intracellular basis of Abeta pathogenicity. *Proc Natl Acad Sci USA* 107(5): 1942-7 (2010).
- [93] Takahashi RH, Milner TA, Li F, Nam EE, Edgar MA, Yamaguchi H, *et al.* Intra-neuronal Alzheimer abeta42 accumulates in multivesicular bodies and is associated with synaptic pathology. *Am J Pathol* 161(5):1869-79 (2002).
- [94] Maezawa I, Hong H-S, Wu H-C, Battina SK, Rana S, Iwamoto T, *et al.* A novel tricyclic pyrone compound ameliorates cell death associated with intracellular amyloid-beta oligomeric complexes. *J Neurochem* 98(1): 57-67 (2006).
- [95] Lu K, Wang J, Hu B, Shi X, Zhou J, Tang Y, *et al.* Brilliant blue G attenuates lipopolysaccharide-mediated microglial activation and inflammation. *Neural Regen Res* 8(7): 599-608 (2013).
- [96] León-Otegui M, Gomez-Villafuertes R, Diaz-Hernandez JI, Diaz-Hernandez M, Miras-Portugal MT, Gualix J. Opposite effects of P2X7 and P2Y2 nucleotide receptors on α -secretase-dependent APP processing in Neuro-2a cells. *FEBS Lett* 585(14): 2255-62 (2011).
- [97] Kroth H, Ansaloni A, Varisco Y, Jan A, Sreenivasachary N, Rezaei-Ghaleh N, *et al.* Discovery and structure activity relationship of small molecule inhibitors of toxic β -amyloid-42 fibril formation. *J Biol Chem* 287(41): 34786-800 (2012).

Received: November 25, 2015

Revised: January 14, 2016

Accepted: January 20, 2016